62
1-15-92 JS ②

PREPARED FOR THE U.S. DEPARTMENT OF ENERGY,
UNDER CONTRACT DE-AC02-76-CHO-3073

PPPL-2784
UC 420, 426, 427

PPPL-2784

TRANSPORT SIMULATIONS OF TFTR: THEORETICALLY-BASED TRANSPORT MODELS AND CURRENT SCALING

BY

M.H. REDI, J.C. CUMMINGS, C.E. BUSH, ET AL.

December 1991

PRINCETON
PLASMA PHYSICS
LABORATORY

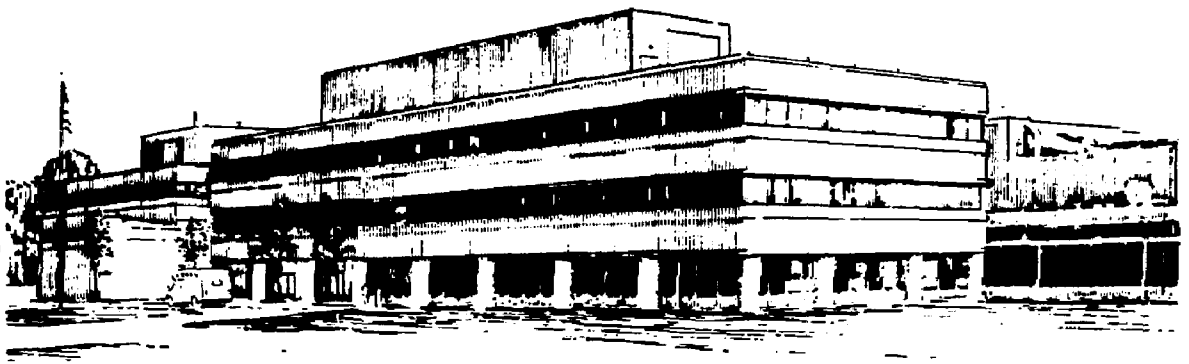

PRINCETON UNIVERSITY, PRINCETON, NEW JERSEY

NOTICE

NOTICE

PPPL--2784

DE92 005130

Transport Simulations of TFTR: Theoretically-Based Transport Models and Current Scaling

M. H. Redi, J. C. Cummings, C. E. Bush, E. Fredrickson,

B. Grek, T. S. Hahm, K. W. Hill, D. W. Johnson,

D. K. Mansfield, H. Park, S. D. Scott, B. C. Stratton,

E. J. Synakowski, W. M. Tang, G. Taylor

Princeton Plasma Physics Laboratory, Princeton University,

Princeton, NJ 08543

Abstract

In order to study the microscopic physics underlying observed L-mode current scaling, 1-1/2-*d* BALDUR has been used to simulate density and temperature profiles for high and low current, neutral beam heated discharges on TFTR with several semi-empirical, theoretically-based models previously compared for TFTR, including several versions of trapped electron drift wave driven transport. Experiments at TFTR, JET and DIII-D show that I_P scaling of τ_E does not arise from edge modes as previously thought, and is most likely to arise from nonlocal processes or from the I_P-dependence of local plasma core transport. Consistent with this, it is found that strong current scaling does not arise from any of several edge models of resistive ballooning. Simulations with the profile consistent drift wave model and with a new model for toroidal collisionless trapped electron mode core transport in a multimode formalism, lead to strong current scaling of τ_E for the L-mode cases on TFTR. None of the theoretically-based models succeeded in simulating the measured temperature and density profiles for **both** high and low current experiments.

(PACS 52.55.Pi, 52.55.Fa, 52.30.Jb, 52.35.Kt)

I. Introduction

Recent research on the basis of plasma confinement has led to the development of several theoretically-based models [1-4] for thermal and particle transport which have been used to simulate experiments on a variety of tokamaks [5-15]. Simulations of TFTR with standardized, benchmarked profile consistent (PCDW) and multimode models have shown that both supershot and L-mode scenarios could not be simulated with a single model [14]. Here L-mode current scaling predictions for TFTR are compared for these theoretically-based models to see if successful predictions can be achieved in this reduced experimental space. In addition to PCDW, we compare the results of TFTR simulations with several different trapped electron mode models within the multimode formulation to measured plasma profiles. Edge transport is provided semiempirically, by a profile-consistent constraint (applied at all radii) or by resistive ballooning modes. The multimode models are tested first for both density and thermal transport predictions. All models are then tested with empirical density transport to provide electron density profiles as measured. Finally, predictions with a recent multimode model, Version 5.10 proposed by Bateman [15] are compared to TFTR measure-

ments.

This paper is organized as follows: In Section II the experiments simulated are discussed. In Section III the models are presented and the transport simulation procedure is briefly described. Results are presented with a discussion in Section IV, and a summary and conclusion is found in Section V.

II. TFTR Experiments Simulated

Two TFTR experiments representing high and low current conditions from a 1989 L-mode current scan [16, 17] are the basis for this comparative study of transport models. The plasma parameters of the high current (I_p = 2.1 MA, shot 45601) and the low current (I_p = 0.9 MA, shot 41087) experiments are shown in Table I. These experiments were chosen for study because most of the externally controlled plasma parameters are very similar, aside from I_P (and q_a). R, a, B_Z, $n_e(r)$, P_{inj}, Z_{eff} are the same, within 15%, for these two experiments. We will compare simulation results to the electron density and temperature profiles, measured by Thomson scattering (shot 41087) and by multichannel infrared interferometry and electron cyclotron

emission (shot 45601) and to ion temperature profiles measured by charge exchange recombination spectroscopy (CHERS), at the end of the neutral beam heating phase. With BALDUR [18, 19, 20] transport simulations of the two TFTR experiments, an approximate estimate of the current scaling exponent ($\tau_E \propto I_p^{\alpha}$) can be made for each transport model.

III. The Theoretical Models and Transport Simulations

A. Theoretically-Based Models

Two types of theoretically-based models for anomalous transport were studied: the profile consistent drift wave model (PCDW), based on trapped electron and η_i transport together with a profile consistency condition providing edge and core transport, and the multimode type [4, 9, 14], made up of the sum of three modes: drift wave (trapped electron and η_i modes), rippling mode and resistive ballooning modes (active at the plasma edge). Both treatments of edge physics may be considered semiempirical since the basis of profile consistency is not understood. Three of the models (PCDW, MM,

MMCD) are exactly as shown in Ref. 14, so that formulations for PCDW and MM may be found in that reference. For clarity, MMCD is described below in detail, because the other models are constructed from the MM and MMCD conceptual framework. In addition to the models for anomalous transport, simplified neoclassical thermal and particle diffusion as well as Ware pinch were included in the simulations [18].

1. PCDW Model

The profile consistent model [1, 5, 14] has proven useful for simulating ohmic and ohmic pellet experiments on several tokamaks [5, 6, 11] and supershot and low power L-mode cases on TFTR [7, 8, 14], but has been found to greatly overestimate ion confinement for high auxiliary heating power in L-mode on TFTR[14] and JET.[13]

2. MM Model

Nine different variants of the multimode formulation have been compared in this study; they differ primarily in the choice of a trapped electron model. Singer's original multimode model (MM)[4] combines a model for trapped electron and η_i losses,[2] with a resistive ballooning model due to Carreras[21]

enhanced by a factor A_3^2.[3] MM has been used successfully to simulate ohmic and L-mode plasmas on ASDEX[4] and TFTR.[14] The heat and particle fluxes are predicted to arise from a combination of drift wave, rippling mode and resistive ballooning modes

$$
\begin{aligned}
Q_e^{ANOM} &= Q_e^{dw} + Q_e^{rm} + Q_e^{rb} \\
Q_i^{ANOM} &= Q_i^{dw} + Q_i^{rm} + Q_i^{rb} \\
\Gamma_a^{ANOM} &= \Gamma_a^{dw} + \Gamma_a^{rm} + \Gamma_a^{rb}.
\end{aligned}
$$

Particle species is designated by subscript a. For drift waves

$$
\begin{aligned}
Q_e^{dw} &= f_e^{dw}(5/2 - 3/2\, f_{ith})\hat{D}_{te}\, f_\beta\, n_e\, \partial T_e/\partial r \\
Q_i^{dw} &= f_i^{dw}\, 5/2(\hat{D}_{te} + f_{ith}\hat{D}_i)\, f_\beta\, n_i\, \partial T_i/\partial r \\
\Gamma_a^{dw} &= f_a^{dw}\, D_a^{dw} n_a/L_n \\
D_a^{dw} &= \frac{1+\beta'/\beta'_{cl}}{1+(\beta'/\beta'_{cl})^3}(1 - \frac{f_{ith}}{0.95+\nu_{ee}})\hat{D}_{te}.
\end{aligned}
$$

For additional details of the MM model, see Ref. 14.

3. MMCD Model

The MMCD model[14] is identical to MM except that the collisionless/dissipative trapped electron mode (CTEM/DTEM) transition

$$D_{te} = (r/R)^{1/2}\omega_e^*/k_\perp^2 min[1, \omega_e^*/\nu_{eff}]$$

is replaced by

$$D_{te} = \epsilon^{1/2}\frac{\omega_e^*}{k_\perp^2}\left[1, \frac{0.1}{\nu_e^*}\right]_{min}$$

following a suggestion by Rewoldt,[23] and the resistive ballooning model is replaced by a more recent resistive ballooning model by Carreras and Diamond.[22] The resistive ballooning model in MMCD also includes pressure driven $\tilde{E} \times \tilde{B}$ flux in χ_e^{rb}, χ_i^{rb} and D^{rb} enhanced by Λ^2, as well as diamagnetic stabilization [24].

$$\begin{aligned}
\chi_e^{rb} &= f_e^{rb}\frac{1}{2^{13/6}\langle n\rangle^{2/3}S^{2/3}\hat{S}}\left(\beta\frac{R_o^2}{L_pR_c}q^2\right)^{4/3}\frac{v_e r^2}{R_o}\Lambda^{4/3}f_{dia} \\
&\quad + f_e^{rb}\frac{\beta R_o^2 q^2}{\sqrt{2}L_pR_cS}\frac{r^2}{\tau_R}\Lambda^2 f_{dia}, \\
D^{rb} &= f_a^{rb}\frac{\beta R_o^2 q^2}{\sqrt{2}L_pR_cS}\frac{r^2}{\tau_R}\Lambda^2 f_{dia}.
\end{aligned}$$

The ion thermal diffusivity is proportional to the particle diffusivity

$$\chi_i^{rb} = f_i^{rb}\frac{\beta R_o^2 q^2}{\sqrt{2}L_pR_cS}\frac{r^2}{\tau_R}\Lambda^2 f^{dia}.$$

Here, the diamagnetic stabilization term is approximated by

$$f_{dia} = \left[1 - \left(\frac{\mu_o \omega_{ci} \rho_i^3}{\eta \beta q^2 L_{ni}}\right)^2\right]^{-1/8}.$$

$\hat{S}$ is the plasma shear. The magnetic Reynold's number is defined by S $= \tau_R/\tau_{hp}, \tau_R = r^2\mu_0/\eta \equiv$ local resistive time, with η = the local Spitzer resistivity and $\tau_{hp} = R_o/v_A \equiv$ local poloidal Alfven time.

4. MMHT, MMHT/no η_i, MMHT/ν_{*e}, MMHT/KP Models

We designate MMHT as the multimode model based on MMCD with a new toroidal collisionless trapped electron model due to Hahm and Tang [25, 26] which replaces the trapped electron part of drift wave mode transport in the model. MMHT refers to results with the multimode model with η_i losses formulated as in MM and MMCD.

$$Q_{e,i}^{dw} = Q_{e,i}^{te} + Q_{e,i}^{\eta_i}$$

with

$$Q_e^{\eta_i} = f_e^{dw}(-3/2 f_{ith}) \hat{D}_{te} f_\beta n_e \partial T_e/\partial r$$

$$Q_i^{\eta_i} = f_i^{dw}(-5/2 f_{ith}) \hat{D}_i f_\beta n_i \partial T_i/\partial r$$

Particle and energy fluxes are now given by

$$\Gamma_e^{te} = -\frac{C_{et}}{G^5}\left(\frac{R}{L_n}\right)^5\left(\frac{R}{GL_n}-\frac{3}{2}\right)^2 exp(-\frac{2R}{GL_n})[\left(\frac{R}{L_n}\right)^{1/2} - log\left(\frac{R}{L_n}\right)^{1/2} - 1]$$

$$\times \frac{(\eta_e T_e/T_i)q^2/\hat{s}^2}{(1+5/4\,\eta_i)(1+(T_i/T_e)(1+\eta_i))^{1/2}}\,\frac{cT_e}{eB_0}\,\frac{\rho_s}{L_{Tr}}\left(\frac{\partial n_e}{\partial r}\right)$$

$$Q_e^{te} = \left(\frac{R}{GL_n}\right)T_e\Gamma_e^{te}$$

$$Q_i^{te} = 2.75(1+1.93\eta_i)(1+1.25\eta_i)^{-1}T_i\Gamma_e^{te}$$

where we take G = 1.2 and C_e = 10. The anomalous electron-ion energy exchange in this model is

$$\Delta^{dw} = \frac{T_e}{L_n}\Gamma^{te}$$

The validity regime of the CTEM weak turbulence theory [25, 26] is

$$v_{Hahm} = 2\left(\frac{2\pi r}{R}\right)^{1/2}\left(\frac{R}{L_nG}\right)^{3/2}\left(\eta_e\frac{R}{L_nG}-3/2\right)\,exp(-\frac{R}{L_nG}) < 1$$

$\hat{D}_{te}$ is given by

$$\hat{D}_{te} = \left(\frac{2^7}{15}\right)[\left(\frac{R}{L_n}\right)^{1/2} - log\left(\frac{R}{L_n}\right)^{1/2} - 1]\left(\frac{R}{L_n}\right)^2\left(\frac{v_{Hahm}^2}{8\pi\eta_e}\right)$$
$$\left(\frac{T_e}{T_i}\right)\left(\frac{(q/\hat{S})^2}{1+1.25\eta_i}\right)\left(1+\frac{T_i}{T_e}(1+\eta_i)\right)^{-1/2}(L_r\omega_e/k_\perp)(\rho_s/L_{Te})$$

Since the Hahm-Tang model for toroidal collisionless trapped electron mode transport is derived for η_i modes being subdominant, simulations were also done without η_i mode losses. This model is designated MMHT/no η_i.

Simulations were also carried out with the Rewoldt ν_{*e} transition from collisionless to dissipative electrons (see Section III.A.3). This model is designated MMHT/ν_{*e}.

For simulations with DTEM provided by the Kadomtsev-Pogutsev model[27]

$$\hat{D}_{te} = \epsilon^{3/2}\eta_e \frac{\omega_e^*}{k_\perp^2}\frac{\omega_e^*}{\nu_{ei}}$$

the model was designated MMHT/KP.

5. MMKP, MMKP/ν_{*e} Models

Simulations were also carried out for Kadomtsev-Pogutsev trapped electron losses with η_i losses as in the MM, MMCD models and with no transition to CTEM (MMKP), as well as to see the effect of the MMKP model with an "inverse" Rewoldt transition to provide CTEM losses (MMKP/ν_{*e}).

6. Version 5.10 Model

Bateman has optimized the multimode model denoted Version 5.10 [15], also based on the MMCD model. It includes the Horton-Hamaguchi η_i mode. Electron drift wave losses are reduced, while resistive ballooning losses are increased by a multiplicative factor 4, relative to the MM and MMCD models.

Diamagnetic stabilization is also significantly reduced, in that the second term in f_{dia} (Section III.A.3) is multiplied by 0.01. See Ref. 15 for further details.

B. Transport Simulations

This section details transport modelling assumptions for all simulations except those for Version 5.10, which are modelled as in Ref. 15 (see Sec. IV.D below). The 1-1/2-d BALDUR code (version 19.09/Cummings,PPPL) was used for simulations of PCDW and multimode models, described in Sections III.A.1-III.A.5. 2-d plasma equilibria were calculated with the Lao VMOMS code.[28] The validity of the electron collisionality condition for each of the theoretical models, is discussed in Section IV.A for each experiment.

1. Simulations with Theoretically-based Particle Transport

The experimental plasma discharges were simulated through the end of neutral beam injection beginning with the ohmic phase. The initial ohmic phase line average electron density was obtained from multiple infrared interferometer (MIRI) measurements. The carbon density was assumed constant

throughout the experiment, with Z_{eff} during neutral beam heating obtained from visible bremsstrahlung. The simulated line average electron density was feedback controlled during the ohmic phase to follow the experimental data. For these L-mode experiments, the ohmic phase lasted 3.5 seconds followed by one second of high power neutral beam injection. The maximum beam energy in both cases was 98 keV with the (full, half, and one-third energy) beam particle fractions being (0.46, 0.28, 0.26). Experimental measurements and BALDUR predictions are compared at the end of the neutral beam phase when the plasma was in steady state.

As shown in Table I, the two experiments are very similar except for the plasma current. They are also similar in impurity-related effects. The fraction of power radiated to input heating power was 22% (24%) for the simulations of shot 45601 (41087). The plasma simulations included 56% (33%) carbon, N_C/N_e, in the ohmic phase dropping to 14% (12%) carbon in the L-mode phase. There is considerable uncertainty about the percentage of radiated power in shot 41087, which developed a small marfe. Simulations with the radiation fraction set to 55% did not change the overall conclusions of this paper since most radiation is at the plasma edge.

Density profiles were evolved for both deuterium and carbon. At the plasma edge the electron and ion temperatures were set to 200 eV and the deuterium (carbon) densities were set to $0.53 \times 10^{19}/m^3$ ($0.12 \times 10^{19}/m^3$).

Recycling was 0.9 throughout.[29] Neoclassical resistivity and a Kadomtsev sawtooth model were used. Sawteeth occurred every 50 ms before neutral beam heating and every 220 (127) ms afterwards for shot 45601 (41087) as in the experiments. Input to the code allowed the number and phase of sawteeth in the neutral beam heated phase to be adjusted to agree with soft x-ray measurements in the two experiments. In the low current experiment the sawtooth radius was reduced and the sawtooth period was about half that of the high current experiment; consequently sawteeth had less effect on overall plasma transport at low current.

The 0.92 m minor radius was divided into 40 radial zones and scale lengths of L_{ne}, L_{Te}, etc. were calculated after smoothing over 12 nearby zones. Maximum scale lengths for n_e, n_i, T_i, T_e, and pressure were set to half the major radius to prevent instabilities in calculating the strongly scale length-dependent transport of MMHT. The radial size for smoothing and the maximum scale lengths were chosen because at lower values the strong

density dependence of the Hahm-Tang CTEM model led to numerical instabilities. Except for MMHT-based models, particle fluxes were calculated using the relation between Γ and D_a^{dw}. For MMHT-based models, f_β was set equal to 1 and $f_{ith} = 0$, unless η_i mode transport was included.

Initial normalization factors used for the multimode models were benchmarked by Ghanem [9], $[f_{i,e,a}^{dw}, f_{i,e,a}^{rm}, f_{i,e,a}^{rb}] = [0.3, 3.0, 1.0]$.

All models overestimated $\tilde{n}_e$ by 20-30% initially. Thus the Ghanem calibration for particle transport from these modes was too high. Simulations were then carried out with the normalization factors $[f_{i,e,a}^{dw}, \ldots]$ scaled up uniformly, by factors of 6-12, to achieve a line averaged density in the range observed for both experiments.

2. Simulations with Empirical Particle Transport

The PCDW simulations used numerical factors benchmarked from BALDUR simulations of several tokamaks by Redi [5-8,14], $[C_F, C_G, C_H] = [0.78, 0.33, 0.5]$. For simulations with the profile consistent model, the plasma density is evolved with an empirical particle transport model to agree with experiment [5-8, 14]. Energy flows of 3/2 kT are associated with particle transport

in the plasma with PCDW. Energy flow associated with particle transport is included implicitly in Q_e and Q_i in the multimode formulation [4, 9, 14].

Since none of the multimode models were found to yield good plasma profiles for n_e, T_e, and T_i (Figs. 1, 2), the theoretically-based models for thermal transport were then tested separately by using empirical density transport coefficients to reproduce the measured electron density within 10%. These simulations with empirical density transport models did not require extra smoothing in calculating the density gradients for evaluating the theoretical models. No such smoothing is applied in these simulations. However, instabilities arising in temperature prediction (with MMHT-based models) were dealt with by limiting the minimum radial temperature scale length to the poloidal ion gyroradius. Use of a larger minimum scale length can not be justified theoretically.

IV. Results and Discussion

The BALDUR simulation results with both types of particle transport models are shown in Tables II-V. The measured central temperatures, the total thermal energy confinement times, the stored energies of thermal elec-

trons and ions and the line averaged electron densities are shown for comparison. The experimental values are taken from SNAP '30' try 18 for shot 41087 and from SNAP try 3 for shot 45601. The SNAP analyses show that the integrated profiles matched the measured stored energy within 10% and the calculated neutron flux was matched within 20%. In Figs. 1-6 are shown the plasma profiles from simulations of the two experiments for models MMCD, MMHT with scaled theoretical particle transport, and for MMCD, MMHT, PCDW and Version 5.10 with empirical particle transport.

A. Simulation Results with Scaled Theoretically-based Transport Models

1. Particle Transport

Using multiplicative factors of 6-12 it was possible to simulate the line averaged electron density of the low current case (within 10%) with all of the theoretically-based models. It was not possible to use the same factors to simulate the line averaged electron density (within 10%) for the high current case with the MMHT and MMHT/ν_{ee} models.

Figures 1 and 2 show the density profiles evolved by the MMCD and

MMHT models, with these scaling factors to increase transport. Edge densities are high in these cases because the theoretical models prescribe identical transport for deuterium and carbon. Thus $n_C(r)$ is flat and in order to achieve the high Z_{eff} of the experiments it was necessary to use a high carbon edge density in the simulations.

The effect of edge resistive ballooning transport on density evolution is small; this mode primarily affects χ_e. Since the density profiles are broader than the temperature profiles, simulations do not require strong edge particle losses. Hulse[32] has modelled TFTR pellet fuelled density profiles with a time-dependent code and a drift-wave like transport model, obtained initially from analysis of gas puff experiments by Efthimion.[33] In these cases, also, particle transport modeling did not require strong edge losses for successful simulation of the TFTR experiments.

2. Thermal Transport

In Tables II and III it is seen that at high current the multimode models underestimate the central plasma temperatures by about a factor of two, except for the MMHT/no η_i model which overestimates T_{io} by a factor of two. Most of the models were able to simulate the central temperatures and

confinement times within 30% for the low current case. Again the MMHT/no η_i model overestimates the ion temperatures, and hence the confinement time.

The stored thermal energies for electrons and ions are seen to be in a ratio of about 3/2 (high current) and 2/1 (low current). Most of the models predict greater stored energy in the electrons than in the ions, except for the MMHT/no η_i model. Such comparisons of stored thermal energy are important in evaluating the predictions of theoretical models for confinement. The experimental measure of τ_E from the SNAP code is obtained by dividing the total stored thermal energy by the calculated power sources while the BALDUR simulated τ_E is obtained by dividing the predicted total stored energy by the calculated power losses at the time of interest. Thus the confinement times are both calculated quantities, converging in steady state. A comparison of plasma stored energies more accurately provides a comparison of modelled to measured energy confinement. We concentrate on I_P scaling of τ_E because most fusion/plasma physics research emphasizes this parameter.

Figures 1 and 2 show the plasma profiles evolved by two of the models, MMCD and MMHT.

The two experiments simulated were chosen because of their overall similarity. However, one difference between these cases is in collisionality. Plots of ν_{*e} show that ν_{*e} is below 0.1 for shot 45601 over most of the plasma interior, a/20 < r < 2/3 a, but does not fall below 0.3 at any radius for low current shot 41087. MMHT and MMHT/no η_i are models with only collisionless trapped electron driven transport and are not valid for the experimental conditions of shot 41087. MMKP has only dissipative trapped electron transport and so is not valid for simulation of shot 45601. In Tables II-V, cases for which the collisionality assumption is outside the experimental range are identified. It happens that the validity condition for the MMHT/no η_i model is satisfied for r<a/2 for the simulations, since the simulated temperatures are greater than measured at low current.

Simulation results at low current for MMHT/KP, MMKP and MMKP/ν_{*e} are identical for both theoretically-based and empirical particle transport. In the low current case, the Kadomtsev-Pogutse DTEM model controls trapped electron driven losses in these three models.

B. Simulation Results with Empirical Particle Transport Models

Tables IV and V show simulation results with empirical particle transport models, using theoretically-based models for thermal transport as described in Section III. The MMHT/no η_i model consistently overpredicts ion temperatures. At high current all other models except PCDW are found to predict the central temperatures and confinement times within 25%. However, at low current the ion temperatures predicted are at least 50% higher than observed and thermal confinement times are also higher, except for PCDW and Version 5.10. Except for the MMHT/no η_i model, the MM, MMCD, MMHT-based and MMKP-based models lead to similar predictions for τ_E for both low and high current. Changing the trapped electron part of these multimode models does not significantly change the predictions when density transport is modelled empirically.

Figures 3-6 show profiles for four of the theoretically-based models, with empirically modelled density profiles. Better simulations would require enhancement of ion energy losses at low current for all models tested.

In Figs. 7 and 8 are shown the relative contributions from each mode to

χ_e and χ_i for MMCD and MMHT, with empirical density transport models. For the high current case, resistive ballooning contributes little to the thermal diffusivities at the plasma edge (Fig. 7a, 7c, 8a, 8c), but at low current the model leads to significant losses there (Fig. 7b, 8b) for χ_e only.

1. Model Optimization

Use of the toroidal CTEM model (MMHT) does improve the electron temperature profiles, compared to MM and MMCD, although at high current a steep T_e gradient develops due to the L_{T_e}-dependence of the coefficients. Smoothing or a larger theory-based minimum L_{T_e} would improve the shape of the predicted electron temperature profile.

While multiplicative factors (0.5, 2.0) could be found for the PCDW χ_e and χ_i models to give significantly better agreement for the high and low current central temperatures, the same factors did not lead to better agreement with experiment for the TFTR L-mode case 41326, simulated with PCDW in Ref. 14.

The electron temperature profiles show clear q dependent profile differences, being narrower at low current. This is the basis of the profile con-

sistency ansatz for the PCDW model. The ion temperature profiles do not show this profile consistent feature so strongly; the PCDW model should be reformulated to apply to typical tokamak ion temperature profiles.

Section IV.D discusses results with a model in which the q dependence of the resistive ballooning mode and overall ion losses are increased empirically. Another way to rectify inadequate ion energy losses at low current might be by an η_i mode model which sufficiently increased η_i transport at low current. In considering effects of theoretical modes, not yet included, which may be active in the experiment, we note that Zarnstorff *et al.*[31] has found that low I_p plasmas at TFTR are not typically characterized by flatter density profiles. Thus stronger η_i losses are not generally expected at low current.

C. Current Scaling

In Tables VI and VII are shown an estimate of the I_p scaling in τ_E obtained for each model, with theoretically-based and empirical particle transport. These are rough estimates, assuming $\tau_E^{th} = AI^{\alpha}$ where A is assumed not to vary between the two experiments. These TFTR experiments exhibit current scaling with $\alpha = 0.88$.

With scaled theoretically-based particle transport, the MM model gives current scaling of $\alpha = 0.67$ compared to MMCD, which used an improved calculation of resistive ballooning and predicts weaker current scaling ($\alpha = 0.44$)! Since the new resistive ballooning model is expected to be closer to the correct physics and and it is widely believed that current scaling may be due to resistive ballooning losses, it is a surprise that the current scaling feature is not preserved in the newer model. Strong current scaling of τ_E is obtained only from the MMHT-based models.

Table VII shows the current scaling exponent of τ_E obtained with empirical models for density transport. The PCDW model is the only model which predicts strong current scaling ($\tau_E \simeq I_P^{1.11}$). The strong current scaling of the MMHT-based models seen with theoretical density transport models, disappears when empirical density transport modelling is used. Thus most of those models' success in predicting confinement time current scaling is due to a strong I_P dependence in the effect of the CTEM particle transport coefficients. These coefficients affect τ_E directly through the density profile and indirectly through the temperature profiles, since thermal losses depend sensitively on L_n in this model. In contrast to the theoretical density mod-

elling results, TFTR data does not show any I_p dependence of density profile shape so that particle transport is not expected to be strongly I_p-dependent. Simulations with smoothing as used for the scaled theoretical model simulations and with increased thermal transport as in those simulations, do not increase the current scaling exponent found for the MMHT model when empirical density modelling is used.

Recent work on the scaling of global energy confinement for high temperature plasmas has focussed on whether the underlying physics is Bohm-like or gyro-Bohm-like [36, 37, 38]. This has important consequences for ignition in future reactors like BPX and ITER, since gyroBohm transport leads to better energy confinement. Experiments indicate Bohm-like transport, while microinstability-based theories indicate gyroBohm-like transport should be expected. The MMCD model treats edge transport with resistive ballooning modes which include both Bohm-like (magnetic fluctuation part) and gyroBohm-like ($E \times B$ part) terms in the transport coefficients. The simulations in this study show that the gyroBohm part is 1/10th the size of the Bohm-like part in χ_e, so that these multimode simulations cannot be used to support gyroBohm transport as dominant in L-mode current scaling at

TFTR.

D. Simulation Results with Version 5.10

Bateman[15] in studying multimode models with several q-dependent models for η_i mode losses, has optimized normalization factors for an MMCD-based model. He finds current scaling for certain TFTR L-mode experiments can be predicted with a multimode model (called Version 5.10) which includes the Horton-Hamaguchi[39] η_i mode and a modified resistive ballooning model.

The effect of this modification of the MMCD resistive ballooning model can be seen by comparing simulations of TFTR shot 41326 with both models. When simulations of shot 41326 with MMCD [14] are compared with those of shot 41326 from Ref. [15], it is found that the modified model causes χ_e^{rb} at the plasma edge to increase by a factor of 4 and χ_i^{rb} to increase by a factor of 30.

Since reference 15 makes strong claims for the usefulness of the Version 5.10 multimode approach, notably for reproducing TFTR L-mode temperature profiles, we have used the identical code (BALDUR version 18.87/Bateman,PPPL) and model as in Ref. 15 to model shots 41087 and 45601. For

ease of comparison, the transport modelling assumptions and empirical density modelling used for testing the Version 5.10 model were just as in Ref. [15].

The simulation results are shown in Tables IV, V and VII and in Figure 6. In contrast to the simulated temperature profiles shown in Ref. [15], Version 5.10 does not succeed in simulating both electron and ion temperature profiles for either of these TFTR experiments. At high current the electron temperature predicted is lower than observed and at low current the ion temperature predicted is higher than observed. In addition the predicted current scaling behavior is closer to $\sqrt{I_P}$ than to I_P. The current scaling exponent found for this model is 0.57; strong current scaling of τ_E is not found with Version 5.10.

There are significant differences between the low and high current cases in this simulation study and in Ref. 15. TFTR shots 45966/45980, the low and high current cases simulated in [15], exhibit central temperatures which do not vary with current, unlike the present cases 41087/45601 for which there is a factor 1.5-2.7 difference; the high current case having higher plasma temperatures. Shots 45966/45980 show density profile peaking which

increases by 8% as current increases by a factor of two. Shots 41087/45601 do not show any current dependence of the density profile peaking as measured by the ratio of central to line averaged electron density. The high/low current TFTR simulations in Ref. 15 led to τ_E scaling with current with $\alpha = 0.94$.

Figure 9 shows the measured total diamagnetic stored energy as a function of plasma current from a database of TFTR L-mode experiments (XP109). This plot of stored energies (points marked by X) has been constrained with neutral beam power from 10 to 15 MW and with line averaged densities from 2.7 to 3.3 $\times 10^{19}/m^3$. Also plotted as circles are the measured total diamagnetic stored energies for shots 41087 and 45601. The squares denote points for shots 45980 and 45866. It is evident that the cases simulated in Ref. 15 are not representative of the strong current scaling shown by the envelope of the best cases.

It is seen then that the choice of particular low/high current TFTR experiments can affect predictions for current scaling from different transport models. The simulation results show clearly that extensive database comparisons are needed to validate a definitive transport model for L-mode predictive simulations.

Results with Version 5.10 might encourage further modification of the edge resistive ballooning model to provide stronger q-dependent transport. The resistive ballooning mode is thought to be unstable but of low growth rate near the plasma edge of high temperature tokamaks [35]. Resistive ballooning modes increase plasma transport when the ratio of the resistive time to the Alfven time is small, when resistive diffusion of the magnetic field and magnetic fluctuations are likely to be large. Empirical enhancement of resistive ballooning transport near the edge must be justified theoretically.

In addition, recent experiments have shown that plasma edge transport is not locally dependent on edge q. In current ramp experiments on TFTR, Zarnstorff *et al.*[40] have demonstrated that global I_p-dependence of transport does not appear to arise from edge localized q-dependent modes. Similar results have been found on JET[41] and DIII-D.[42] Hence modification of resistive ballooning edge transport in tokamaks to give current scaling does not appear valid even as a semi-empirical construct.

V. Conclusion

1-1/2-d transport simulations of TFTR L-mode experiments have been carried out to test current scaling predictions of theoretically-based models for particle and energy loss processes in tokamaks.

It has often been suggested that the current (I_P) scaling observed in auxiliary-heated L-mode type discharges is primarily caused by resistive ballooning modes in the edge region of tokamaks. Recent experiments however suggest that the I_P dependence of transport is not local to the edge and is likely due to I_P-dependent local core transport or nonlocal transport processes. Consistent with this, our simulations with empirical density modelling show that a) current scaling for the two TFTR experiments simulated is predicted only by the nonlocal PCDW model and b) edge models based on resistive ballooning do not give current scaling for these cases.

Simulations of plasma density and temperature with scaled multimode models based on the Hahm-Tang toroidal CTEM model did lead to current scaling of τ_E for TFTR. However, with empirical density transport modelling no current scaling was predicted with the MMHT-based models. With empirical density transport models, the PCDW and Version 5.10 models predicted

$\tau_E = I_P^{1.11}$ and $\tau_E \sim I_P^{0.57}$, respectively for TFTR. None of the theoretically-based models using either theoretically-based or empirical particle transport, were successful in simulating the plasma density and temperatures profiles for both low and high current cases.

Extrapolation of tokamak performance to a next generation reactor is predicated on I_P scaling of confinement, as seen in both L-mode and H-mode experiments worldwide. These simulations show that present predictive models underestimate ion losses at low current by a factor of 2-4. There remains a challenge to plasma theory to identify an I_P-dependent ion loss mechanism, causing additional transport at low I_P across the plasma not just at the plasma edge, and to develop a self consistent set of toroidal CTEM, DTEM and η_i models for transport simulations of experiment.

Acknowledgment

It is a pleasure to acknowledge discussions with C. Barnes, G. Bateman, K. McGuire, D. R. Mikkelsen, F. W. Perkins, A. T. Ramsey, J. Schivell, C. E. Singer and M. C. Zarnstorff as well as excellent computational support from C. E. Lee. This work was supported by the U.S.Department of Energy

Contract No. DE-AC02-76-CHO-3073.

References

[1]W.M. Tang, Nucl. Fusion **26**, 1605 (1986).

[2]R. Dominguez, R.E. Waltz, Nucl. Fusion **27**. 65 (1987).

[3]J. Sheffield, Nucl Fusion **29**, 1347 (1989).

[4]C.E. Singer, Comments Plasma Phys. Controll. Fusion **11**, 165 (1988).

[5]M.H. Redi, W.M. Tang, P.C. Efthimion, D.R. Mikkelsen, G.L. Schmidt, Nucl. Fusion **27**, 2001 (1987).

[6]M.H. Redi, W.M. Tang, D.K. Owens, M. Greenwald, O. Gruber, M. Kaufmann, Fusion Technol. **18**, 223 (1990).

[7]W.M. Tang, C.M. Bishop, B. Coppi, et al., in Plasma Physics and Controlled Nuclear Fusion Research 1986 (Proc. 11th Int. Conf. Kyoto, 1986), Vol. 1, IAEA, Vienna (1987) 337.

[8]W.M. Tang, N.L. Bretz, T.S. Hahm, et al., in Plasma Physics and Controlled Fusion Research 1988 (Proc. 11th Int. Conf. Nice, 1988), Vol. 2, IAEA, Vienna (1989) 153.

[9]E.S. Ghanem, C.E.Singer, G. Bateman. D.P. Stotler, Nucl. Fusion **30**, 1595 (1990).

[10]F. Romanelli, W.M. Tang, et al., Nucl. Fusion **26**, 1515 (1986).

[11]D. L. Brower, M.H. Redi, W.M. Tang, et al., Nucl. Fusion **29**, 1247 (1986).

[12]A. *Nocentini and* C.G. Schultz, "Transport Studies for Ignition Experiments", Ecole Polytechnique Federal de Lausanne - Suisse Internal Report LRP409/90 (July 1990) 40pp.

[13]A. Taroni, IAEA Workshop on Tokamak Transport, Princeton Plasma Physics Laboratory, October 1990.

[14]M. H. Redi, G. Bateman, Nucl. Fusion **31** 547 (1991).

[15]G. Bateman, C. E. Singer, J. Kinsey, Proceedings of the 18th European Conference on Controlled Fusion and Plasma Physics, Berlin, 1991. G. Bateman, PPPL report 2764, Phys. Fluids, in press.

[16]D.W. Johnson, S.D. Scott, C.W. Barnes, et al., in Controlled Fusion and Plasma Heating (Proc. 17th Eur. Conf. Amsterdam, 1990), Vol. 14B, Part I, European Physical Society, 114 (1990).

[17]S. Scott, V. Arunasalam, C. W. Barnes, M. G. Bell, M. Bitter, et al. 'Correlations of heat and momentum transport in the TFTR tokamak" Phys. Fluids B2(6), 1990, p1300-1305. Physics and Controlled Nuclear Fusion Research, Washington, D.C. October 1990 (paper IAEA-CN-53/A-3-6).

[18]C.E.Singer, D. E. Post, D. R. Mikkelsen, M. H. Redi, A. H. McKenney, Comput. Phys. Commun. **49** (1988) 275.

[19]M. H. Redi, Comput. Phys. Commun. **49** (1988) 399.

[20]G. Bateman 'Simulation of Transport in Tokamaks", pp. 381-401 in Computer Applications in Plasma Science and Engineering, edited by A. T. Drobot (Springer-Verlag, NY, 1991).

[21]B.A. Carreras, P.H. Diamond, M. Murakami, et al., Phys. Rev. Lett. **50**, 503 (1983).

[22]B.A. Carreras, P.H. Diamond, Phys. Fluids B **1**, 1011 (1989).

[23]G. Rewoldt, PPPL, private communication (1989).

[24]B. A. Carreras, ORNL, private communication (1989).

[25]T. S. Hahm, S. C. Cowley, J. Cummings, G. W. Hammett, R. M. Kulsrud, et al. 13th International Conference on Plasma Physics and Controlled Nuclear Fusion Research, Washington, D.C. October 1990 (paper IAEA-CN-53/D-1-1).

[26]T.S. Hahm, W. M. Tang, Phys. Fluids B **3**, 989 (1991).

[27]B. B. Kadomtsev, O. P. Pogutse, Nucl. Fus. 11 (1971) 67.

[28]Lao, L.L., Hirshman, S.P., Wieland, R. M., Phys. Fluids 24 (1981) 1431.

[29]B. Budny, PPPL private communication (1989).

[30]H. Towner, R. Goldston, "On-line transport analysis for TFTR", BAPS, 29, 8 (1984) 1305.

[31]Zarnstorff, PPPL, private communication (1990).

[32]R.A. Hulse, P. Efthimion, G. L. Schmidt, D.K.Owens, H. Park, G. Taylor, 'Nonlinear transport modelingof TFTR Pellet Density Relaxation", Transport Task Force Meeting. Austin, Texas, March 1991.

[33]P. C. Efthimion, D. K. Mansfield, S. Cowley, R. J. Goldston, B. C. Stratton et al, Sherwood Theory Conference, Williamsburg, Va. April, 1990 Paper

2C21.

[34]E. Ghanem, C.E. Singer, BAPS, 35(1990) paper 3Q18.

[35]J. Jakoby, "Nonlinear Resistive MHD Code in Cylindrical Geometry", IPP 6/629 (1987).

[36]R. J. Goldston, BAPS, 34 (1989).

[37]F. W. Perkins, BAPS, 35 (1990).

[38]R. Waltz, BAPS, 35 (1990).

[39]S. Hamaguchi, W.Horton, Phys. Fluids B2 (1990) 1933-1951.

[40]M. Zarnstorff, C. W. Barnes, P. C. Efthimion, G. W. Hammett, W. Horton et al., 13th International Conference on Plasma Physics and Controlled Nuclear Fusion Research, Washington, D.C. October 1990 (paper IAEA-CN-53/A-11-2).

[41]J. G. Cordey, Transport Task Force Meeting, Austin, Texas, March 1991.

[42]J. Ferron, Transport Task Force Meeting, Austin, Texas, March 1991.

Table I. TFTR L-mode Experiments

Shot	45601	41087
R(m)	2.6	2.6
a(m)	0.93	0.92
I_p(MA)	2.1	0.90
B_z(T)	4.5	3.8
$\bar{n}_e(10^{19}m^3)$	3.2	2.9
Z_{eff}	3.3	3.1
P_{inj}	13.2	12.8
q_a	4.6	9.8

Table II. Simulation Results with Scaled

Theoretical Models for Density Transport

SHOT 45601	T_e	T_i	τ_E^{th}	W_e	W_i	$\bar{n}_e$
$q_a = 4.6$	keV	keV	sec	MJ	MJ	$10^{19}/m^3$
Experiment	6.0	7.8	0.084	0.628	0.416	3.2
Models:						
MM	4.1	4.0	0.069	0.636	0.335	3.4
MMCD	3.3	3.4	0.058	0.522	0.320	3.5
MMHT	5.6	4.1	0.082	0.753	0.397	3.7
MMHT/no η_i	8.5	16.9	0.166	1.023	1.298	3.5
MMHT/ν_{ee}	5.6	4.0	0.087	0.811	0.425	3.8
MMHT/KP	3.4	3.2	0.048	0.456	0.257	3.3
MMKP[a]	3.4	3.4	0.048	0.455	0.257	3.4
MMKP/ν_{ee}	3.4	3.3	0.048	0.456	0.259	3.4

[a] This model not valid for experimental ν_{ee}.

Table III. Simulation Results with Scaled

Theoretical Models for Density Transport

SHOT 41087 $q_a = 9.8$	T_e keV	T_i keV	τ_E^{th} sec	W_e MJ	W_i MJ	$\bar{n}_e$ $10^{19}/m^3$
Experiment	4.1	2.9	0.040	0.267	0.158	2.9
Models:						
MM	3.3	3.9	0.039	0.316	0.171	2.6
MMCD	2.9	2.8	0.040	0.303	0.207	3.0
MMHT[a]	3.7	3.1	0.038	0.295	0.187	2.9
MMHT/no η_i[a]	5.1	8.5	0.062	0.380	0.398	2.7
MMHT/ν_{ae}	3.9	3.2	0.047	0.367	0.228	3.0
MMHT/KP	2.8	2.9	0.033	0.257	0.165	2.7
MMKP	2.8	2.9	0.033	0.257	0.165	2.7
MMKP/ν_{ae}	2.8	2.9	0.033	0.257	0.165	2.7

[a] This model not valid for experimental ν_{ae}.

Table IV. Simulation Results with Empirical Models for Density Transport

SHOT 45601	T_e	T_i	τ_E^{th}	W_e	W_i	n_e
q_a = 4.6	keV	keV	sec	MJ	MJ	$10^{19}/m^3$
Experiment	6.0	7.8	0.084	0.628	0.416	3.2
Models:						
PCDW	6.5	9.2	0.136	0.971	0.747	3.5
MM	5.3	6.3	0.106	0.745	0.470	3.2
MMCD	4.6	6.3	0.103	0.721	0.492	3.2
MMHT	6.7	6.1	0.095	0.677	0.469	3.2
MMHT/no η_i	10.0	19.1	0.132	0.820	0.802	3.2
MMHT/ν_{ee}	6.8	6.3	0.102	0.704	0.490	3.2
MMHT/KP	5.0	6.3	0.100	0.685	0.489	3.2
MMKP[a]	5.1	6.7	0.104	0.698	0.502	3.2
MMKP/ν_{ee}	5.4	7.1	0.109	0.748	0.530	3.2
Ver. 5.10	4.8	7.5	0.078	0.565	0.426	3.2

[a]This model not valid for experimental ν_{ee}.

Table V. Simulation Results with Empirical Models for Density Transport

SHOT 41087	T_e	T_i	τ_E^{th}	W_e	W_i	$\bar{n}_e$
q_a = 9.8	keV	keV	sec	MJ	MJ	$10^{19}/m^3$
Experiment	4.1	2.9	0.040	0.267	0.158	2.9
Models:						
PCDW	3.9	5.9	0.053	0.351	0.339	3.0
MM	4.8	4.5	0.091	0.581	0.364	3.0
MMCD	4.2	4.9	0.085	0.543	0.433	3.1
MMHT[a]	5.8	4.4	0.086	0.518	0.382	3.1
MMHT/no η_i	9.9	19.1	0.123	0.690	0.848	3.2
MMHT/ν_{*e}	6.3	4.8	0.087	0.578	0.428	3.1
MMHT/KP	4.4	4.8	0.082	0.522	0.418	3.1
MMKP	4.4	4.8	0.082	0.522	0.418	3.1
MMKP/ν_{*e}	4.4	4.8	0.082	0.522	0.418	3.1
Ver. 5.10	3.6	4.6	0.048	0.357	0.267	3.0

[a]This model not valid for experimental ν_{*e}.

Table VI: Current Scaling Exponent of τ_E

with Scaled Theoretical Models for Density Transport

	α
Exp	0.88
Models:	
MM	0.67
MMCD	0.44
MMHT	0.91
MMHT/no η_i	1.16
MMHT/ν_{ee}	0.73
MMHT/KP	0.44
MMKP	0.44
MMKP/ν_{ee}	0.44

Table VII: Current Scaling Exponent of τ_E with Empirical Models for Density Transport

	α
Exp	0.88
Models:	
PCDW	1.11
MM	0.18
MMCD	0.23
MMHT	0.12
MMHT/no η_i	0.07
MMHT/ν_{*e}	0.19
MMHT/KP	0.23
MMKP	0.28
MMKP/ν_{*e}	0.34
Ver. 5.10	0.57

Figures

FIG. 1. Simulations of electron density and electron and ion temperature profiles compared to measured data from shots 45601 (a, c, e) and 41087 (b, d, f) for the MMCD model; scaled theoretical models include density transport model.

FIG. 2. Simulations of electron density and electron and ion temperature profiles compared to measured data from shots 45601 (a, c, e) and 41087 (b, d, f) for the MMHT model; scaled theoretical models include density transport model.

FIG. 3. Simulations of electron density and electron and ion temperature profiles compared to measured data from shots 45601 (a, c, e) and 41087 (b, d, f) for the MMCD model; empirical density transport.

FIG. 4. Simulations of electron density and electron and ion temperature profiles compared to measured data from shots 45601 (a, c, e) and 41087 (b, d, f) for the MMHT model; empirical density transport.

FIG. 5. Simulations of electron density and electron and ion temperature profiles compared to measured data from shots 45601 (a, c, e) and 41087

(b, d, f) for the PCDW model: empirical density transport.

FIG. 6. Simulations of electron density and electron and ion temperature profiles compared to measured data from shots 45601 (a, c, e) and 41087 (b, d, f) for the Version 5.10 model: empirical density transport.

FIG. 7. Components of χ_e and χ_i for simulations for shots 45601 (a, b) and 41087 (c, d) from trapped electron, η_i and resistive ballooning modes for the MMCD model.

FIG. 8. Components of χ_e and χ_i for simulations for shots 45601 (a, b) and 41087 (c, d) from trapped electron, η_i and resistive ballooning modes for the MMHT model.

FIG. 9. Total measured diamagnetic stored energy as a function of plasma current for TFTR L-mode experiments, constrained to beam power and density as in the text (points marked by X). Circles denote experiments simulated in this paper. Squares denote experiments simulated in Ref. 15.

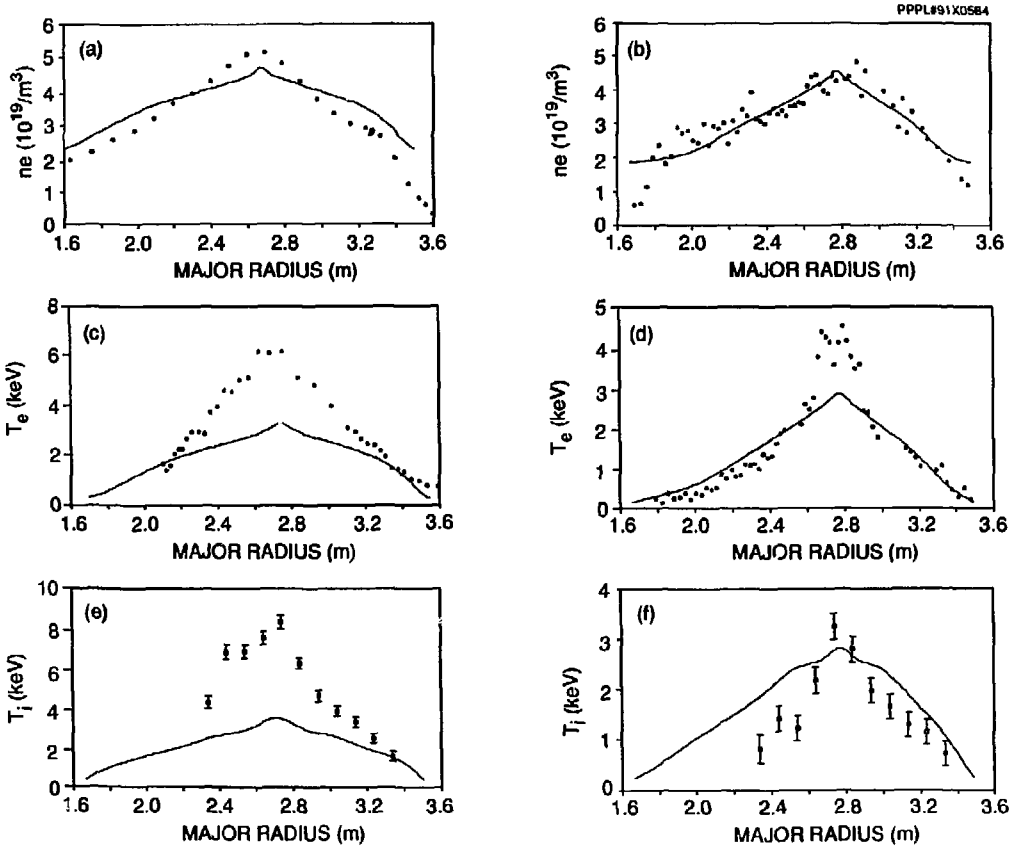
PPPL#91X0584
(a)
ne (10^{19}/m^3)
MAJOR RADIUS (m)
(b)
ne (10^{19}/m^3)
MAJOR RADIUS (m)
(c)
T_e (keV)
MAJOR RADIUS (m)
(d)
T_e (keV)
MAJOR RADIUS (m)
(e)
T_i (keV)
MAJOR RADIUS (m)
(f)
T_i (keV)
MAJOR RADIUS (m)

Fig. 1

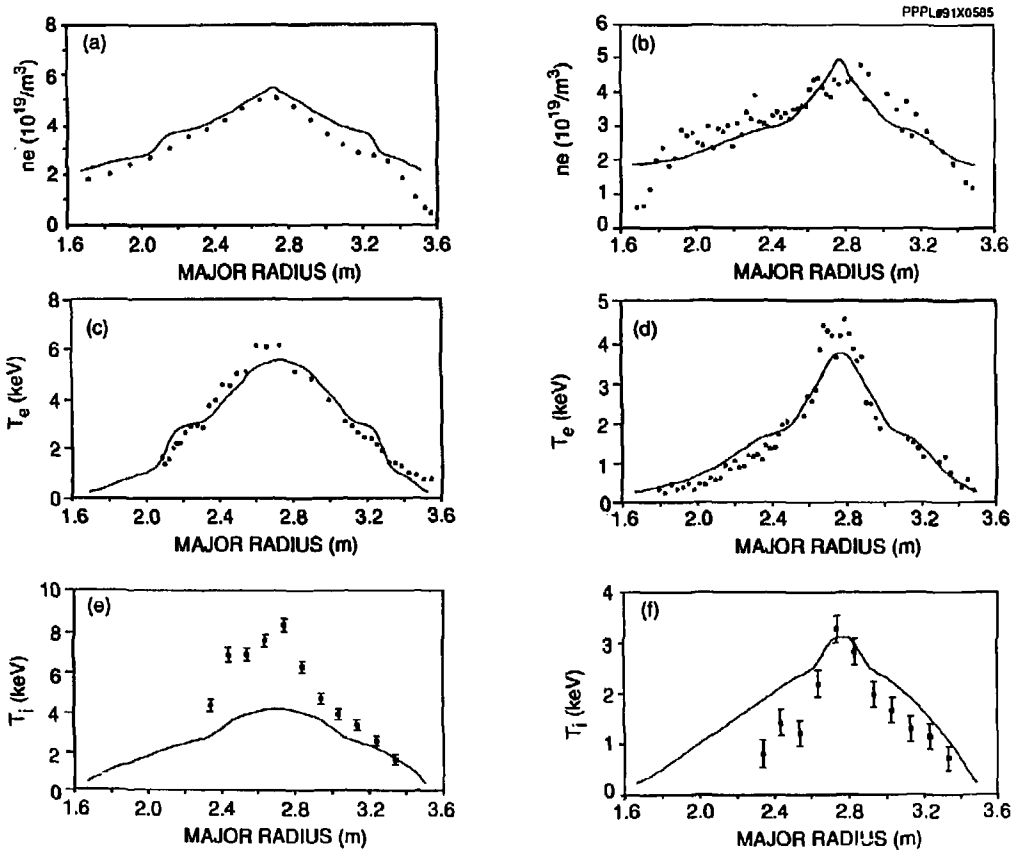
PPPL-91X0585
(a)
ne (10^{19}/m^3)
MAJOR RADIUS (m)
(b)
ne (10^{19}/m^3)
MAJOR RADIUS (m)
(c)
T_e (keV)
MAJOR RADIUS (m)
(d)
T_e (keV)
MAJOR RADIUS (m)
(e)
T_i (keV)
MAJOR RADIUS (m)
(f)
T_i (keV)
MAJOR RADIUS (m)

Fig. 2

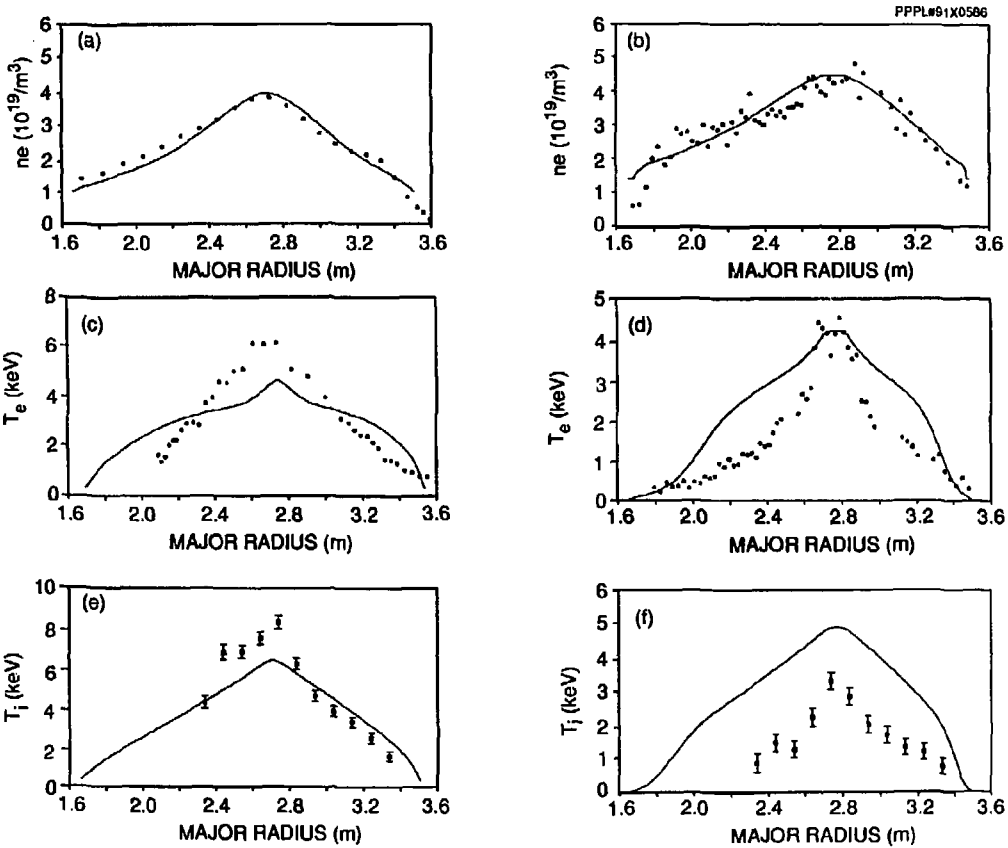
PPPL#91X0586
(a)
ne (10^{19}/m^3)
MAJOR RADIUS (m)
(b)
ne (10^{19}/m^3)
MAJOR RADIUS (m)
(c)
T_e (keV)
MAJOR RADIUS (m)
(d)
T_e (keV)
MAJOR RADIUS (m)
(e)
T_i (keV)
MAJOR RADIUS (m)
(f)
T_i (keV)
MAJOR RADIUS (m)

Fig. 3

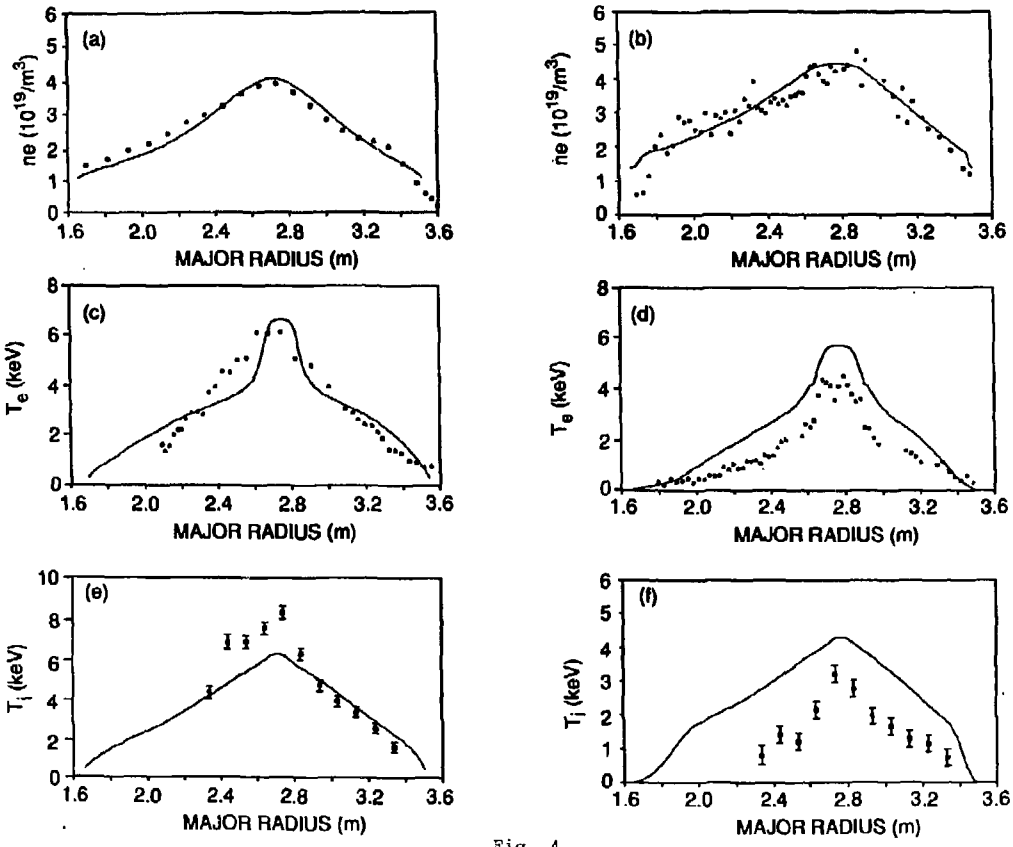
(a)
ne (10^{19}/m^3)
MAJOR RADIUS (m)
(b)
ne (10^{19}/m^3)
MAJOR RADIUS (m)
(c)
T_e (keV)
MAJOR RADIUS (m)
(d)
T_e (keV)
MAJOR RADIUS (m)
(e)
T_i (keV)
MAJOR RADIUS (m)
(f)
T_i (keV)
MAJOR RADIUS (m)

Fig. 4

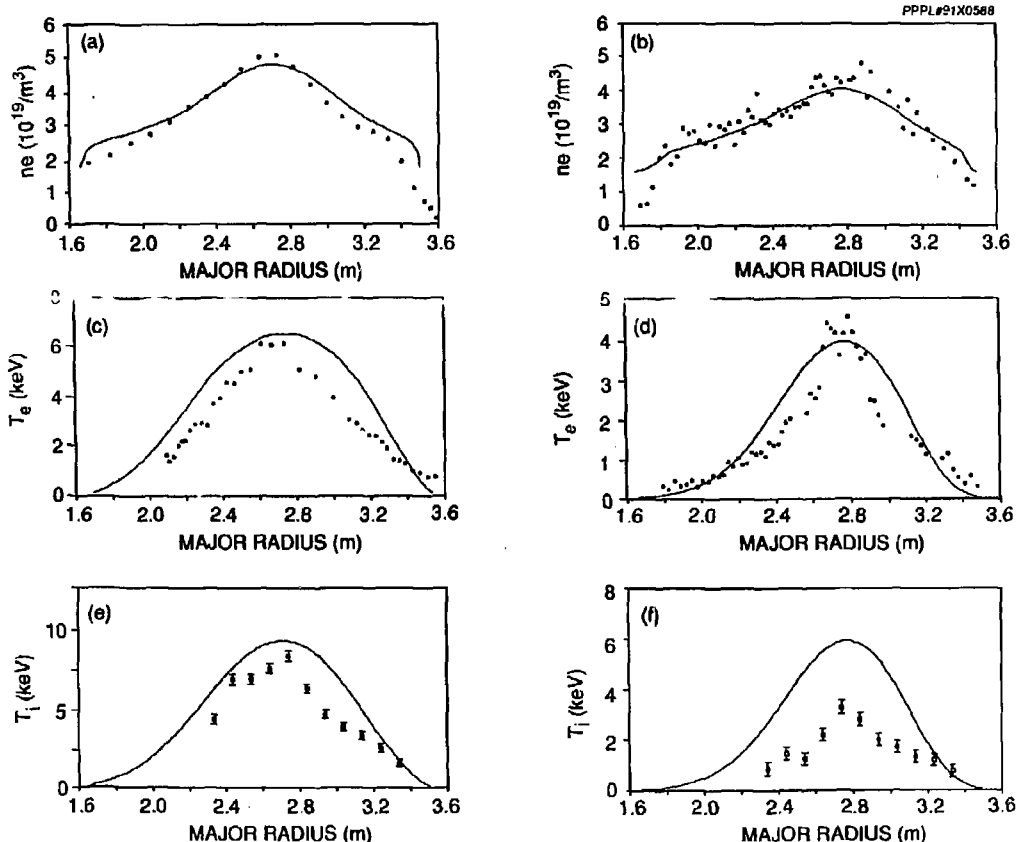
PPPL#91X0588
(a)
ne (10^{19}/m^3)
MAJOR RADIUS (m)
(b)
ne (10^{19}/m^3)
MAJOR RADIUS (m)
(c)
T_e (keV)
MAJOR RADIUS (m)
(d)
T_e (keV)
MAJOR RADIUS (m)
(e)
T_i (keV)
MAJOR RADIUS (m)
(f)
T_i (keV)
MAJOR RADIUS (m)

Fig. 5

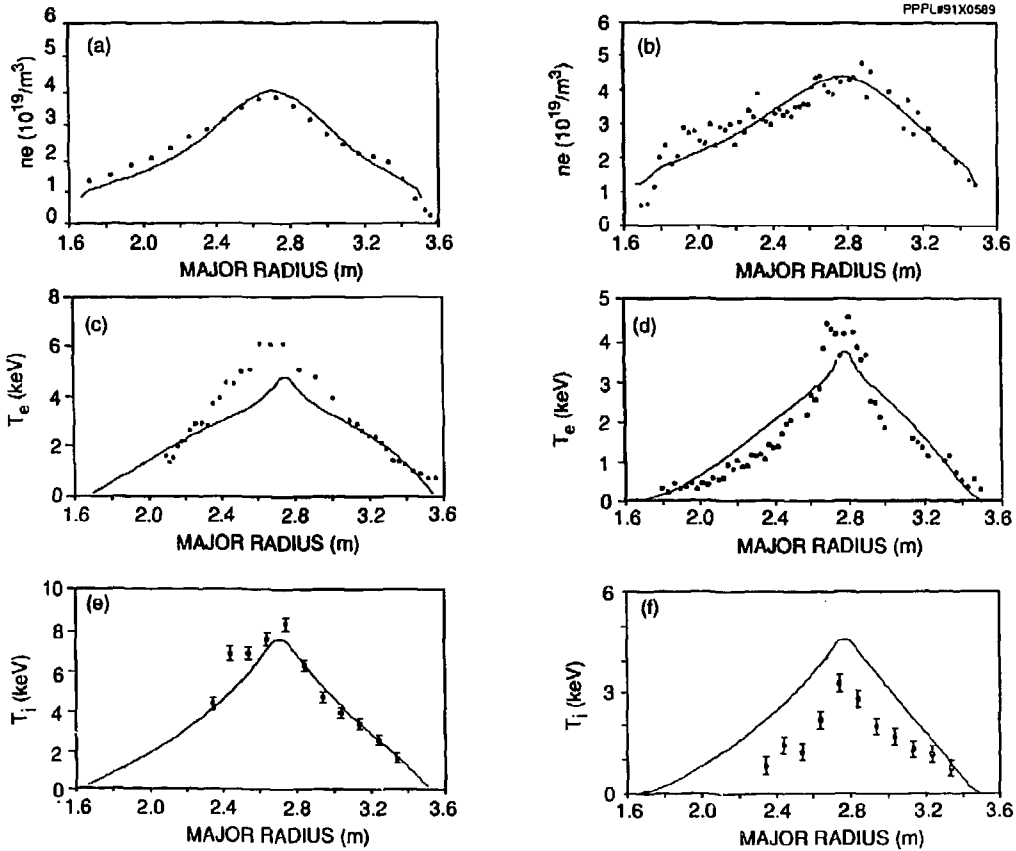
PPPL#91X0589
(a)
ne (10^{19}/m^3)
MAJOR RADIUS (m)
(b)
ne (10^{19}/m^3)
MAJOR RADIUS (m)
(c)
T_e (keV)
MAJOR RADIUS (m)
(d)
T_e (keV)
MAJOR RADIUS (m)
(e)
T_i (keV)
MAJOR RADIUS (m)
(f)
T_i (keV)
MAJOR RADIUS (m)

Fig. 6

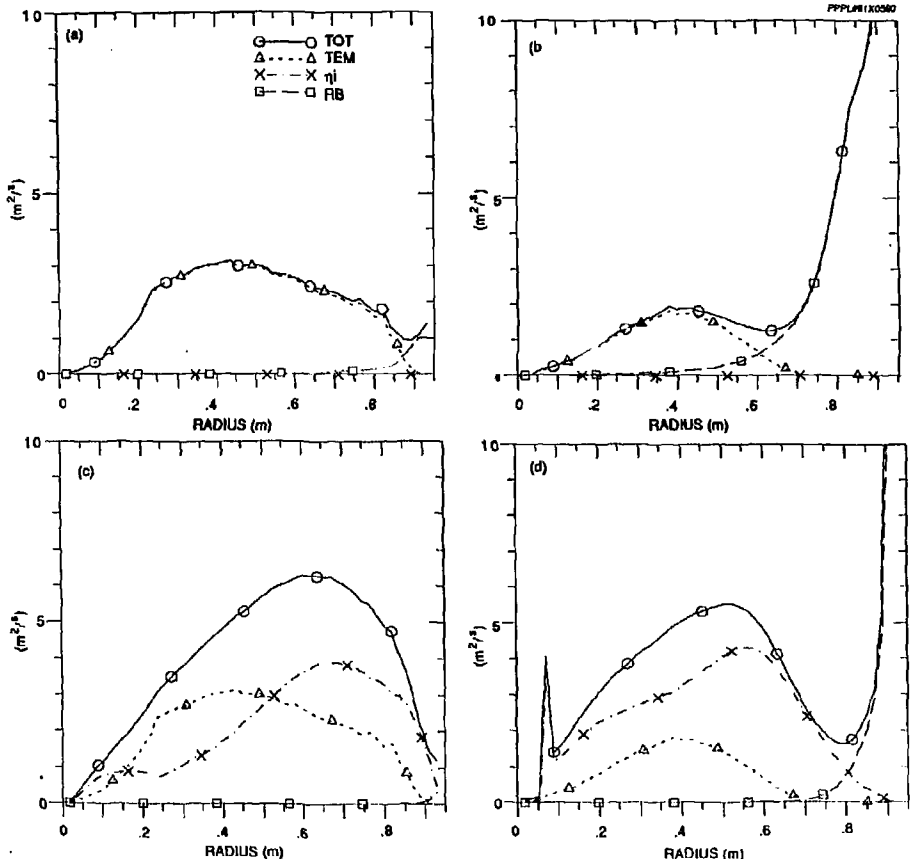

Fig. 7

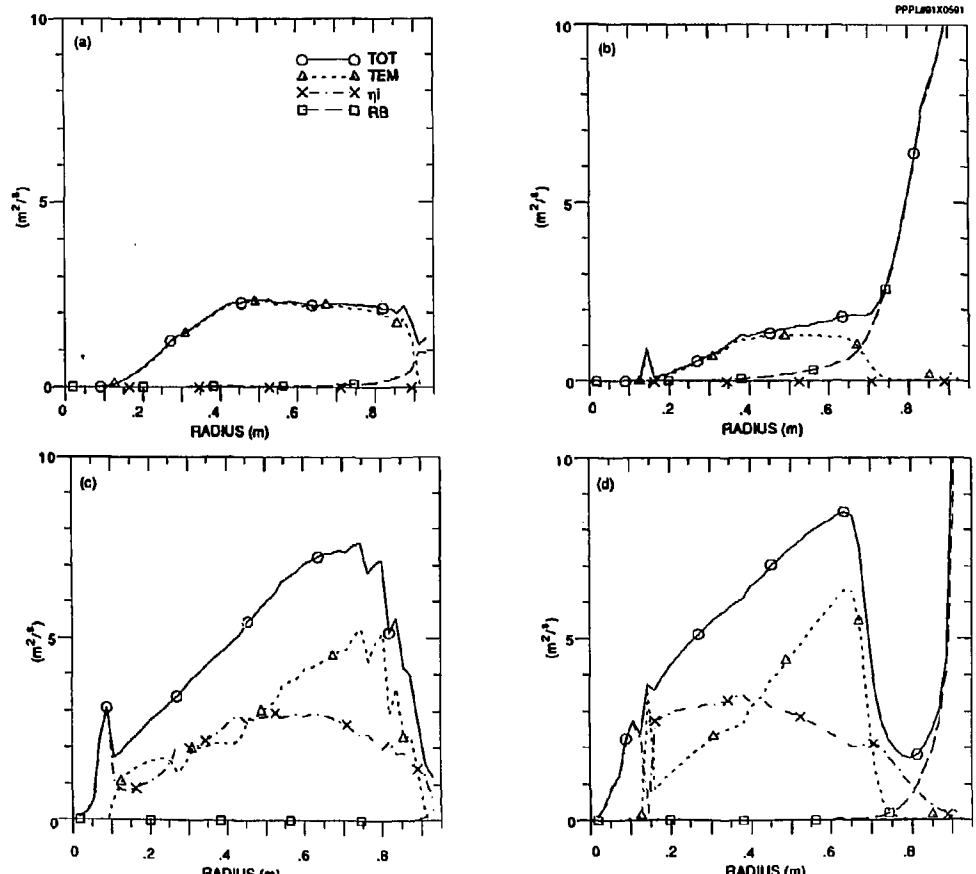

Fig. 8

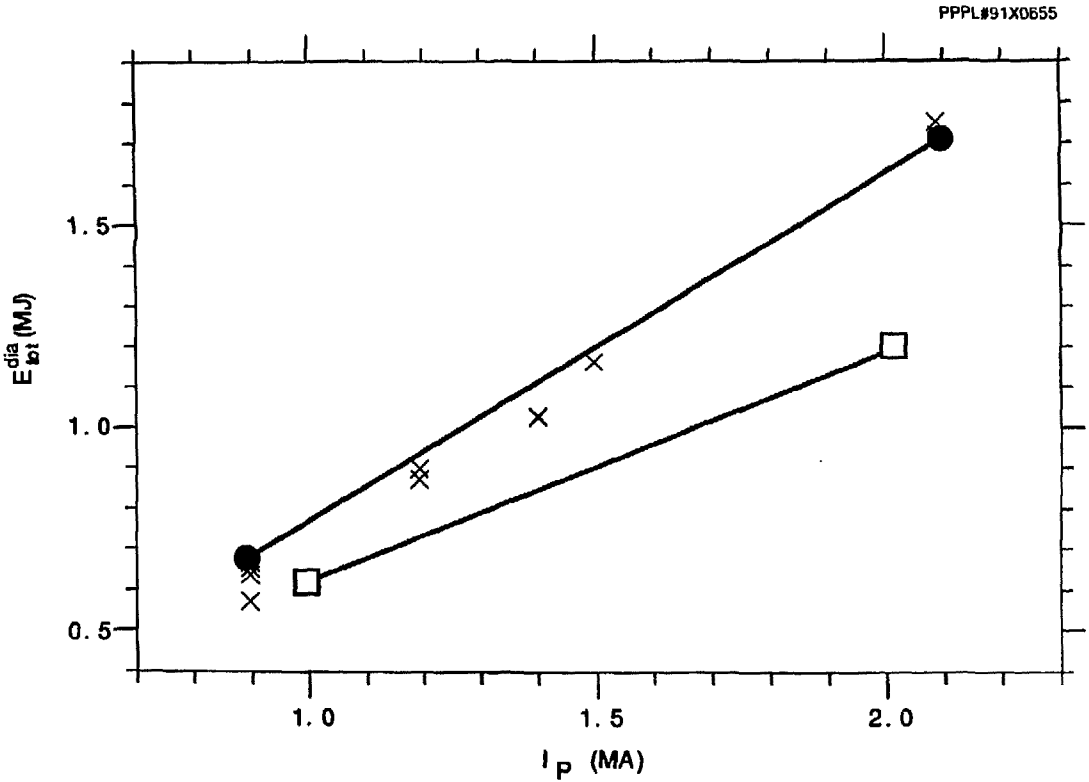

Fig. 9

EXTERNAL DISTRIBUTION IN ADDITION TO UC-420

Dr. F. Paoloni, Univ. of Wollongong, AUSTRALIA
Prof. M.H. Brennan, Univ. of Sydney, AUSTRALIA
Plasma Research Lab., Australian Nat. Univ., AUSTRALIA
Prof. I.R. Jones, Flinders Univ, AUSTRALIA
Prof. F. Cap, Inst. for Theoretical Physics, AUSTRIA
Prof. M. Heindler, Institut für Theoretische Physik, AUSTRIA
Prof. M. Goossens, Astronomisch Instituut, BELGIUM
Ecole Royale Militaire, Lab. de Phy. Plasmas, BELGIUM
Commission-European, DG. XII-Fusion Prog., BELGIUM
Prof. R. Boucique, Rijksuniversiteit Gent, BELGIUM
Dr. P.H. Sakanaka, Instituto Fisica, BRAZIL
Instituto Nacional De Pesquisas Espaciais-INPE, BRAZIL
Documents Office, Atomic Energy of Canada Ltd., CANADA
Dr. M.P. Bachynski, MPB Technologies, Inc., CANADA
Dr. H.M. Skarsgard, Univ. of Saskatchewan, CANADA
Prof. J. Teichmann, Univ. of Montreal, CANADA
Prof. S.R. Sreenivasan, Univ. of Calgary, CANADA
Prof. T.W. Johnston, INRS-Energie, CANADA
Dr. R. Bolton, Centre canadien de fusion magnétique, CANADA
Dr. C.R. James,, Univ. of Alberta, CANADA
Dr. P. Lukác, Komenského Universzita, CZECHO-SLOVAKIA
The Librarian, Culham Laboratory, ENGLAND
Library, R61, Rutherford Appleton Laboratory, ENGLAND
Mrs. S.A. Hutchinson, JET Library, ENGLAND
Dr. S.C. Sharma, Univ. of South Pacific, FIJI ISLANDS
P. Mähönen, Univ. of Helsinki, FINLAND
Prof. M.N. Bussac, Ecole Polytechnique,, FRANCE
C. Mouttet, Lab. de Physique des Milieux Ionisés, FRANCE
J. Radet, CEN/CADARACHE - Bat 506, FRANCE
Prof. E. Economou, Univ. of Crete, GREECE
Ms. C. Rinni, Univ. of Ioannina, GREECE
Dr. T. Mual, Academy Bibliographic Ser., HONG KONG
Preprint Library, Hungarian Academy of Sci., HUNGARY
Dr. B. DasGupta, Saha Inst. of Nuclear Physics, INDIA
Dr. P. Kaw, Inst. for Plasma Research, INDIA
Dr. P. Rosenau, Israel Inst. of Technology, ISRAEL
Librarian, International Center for Theo Physics, ITALY
Miss C. De Palo, Associazione EURATOM-ENEA , ITALY
Dr. G. Grosso, Istituto di Fisica del Plasma, ITALY
Prof. G. Rostangni, Istituto Gas Ionizzati Del Cnr, ITALY
Dr. H. Yamato, Toshiba Res & Devel Center, JAPAN
Prof. I. Kawakami, Hiroshima Univ., JAPAN
Prof. K. Nishikawa, Hiroshima Univ., JAPAN
Director, Japan Atomic Energy Research Inst., JAPAN
Prof. S. Itoh, Kyushu Univ., JAPAN
Research Info. Ctr., National Instit. for Fusion Science, JAPAN
Prof. S. Tanaka, Kyoto Univ., JAPAN
Library, Kyoto Univ., JAPAN
Prof. N. Inoue, Univ. of Tokyo, JAPAN
Secretary, Plasma Section, Electrotechnical Lab., JAPAN
S. Mori, Technical Advisor, JAERI, JAPAN
Dr. O. Mitarai, Kumamoto Inst. of Technology, JAPAN
J. Hyeon-Sook, Korea Atomic Energy Research Inst., KOREA
D.I. Choi, The Korea Adv. Inst. of Sci. & Tech., KOREA
Prof. B.S. Liley, Univ. of Waikato, NEW ZEALAND
Inst of Physics, Chinese Acad Sci PEOPLE'S REP. OF CHINA
Library, Inst. of Plasma Physics, PEOPLE'S REP. OF CHINA
Tsinghua Univ. Library, PEOPLE'S REPUBLIC OF CHINA
Z. Li, S.W. Inst Physics, PEOPLE'S REPUBLIC OF CHINA
Prof. J.A.C. Cabral, Instituto Superior Tecnico, PORTUGAL
Dr. O. Petrus, AL I CUZA Univ., ROMANIA
Dr. J. de Villiers, Fusion Studies, AEC, S. AFRICA
Prof. M.A. Hellberg, Univ. of Natal, S. AFRICA
Prof. D.E. Kim, Pohang Inst. of Sci. & Tech., SO. KOREA
Prof. C.I.E.M.A.T. Fusion Division Library, SPAIN
Dr. L. Stenflo, Univ. of UMEA, SWEDEN
Library, Royal Inst. of Technology, SWEDEN
Prof. H. Wilhelmson, Chalmers Univ. of Tech., SWEDEN
Centre Phys. Des Plasmas, Ecole Polytech, SWITZERLAND
Bibliotheek, Inst. Voor Plasma-Fysica, THE NETHERLANDS
Asst. Prof. Dr. S. Cakir, Middle East Tech. Univ., TURKEY
Dr. V.A. Glukhikh,Sci. Res. Inst. Electrophys.l Apparatus, USSR
Dr. O.D. Ryutov, Siberian Branch of Academy of Sci., USSR
Dr. G.A. Eliseev, I.V. Kurchatov Inst., USSR
Librarian, The Ukr.SSR Academy of Sciences, USSR
Dr. L.M. Kovrizhnykh, Inst. of General Physics, USSR
Kernforschungsanlage GmbH, Zentralbibliothek, W. GERMANY
Bibliothek, Inst. Für Plasmaforschung, W. GERMANY
Prof. K. Schindler, Ruhr-Universität Bochum, W. GERMANY
Dr. F. Wagner, (ASDEX), Max-Planck-Institut, W. GERMANY
Librarian, Max-Planck-Institut, W. GERMANY
Prof. R.K. Janev, Inst. of Physics, YUGOSLAVIA